



Final Draft **of the original manuscript**

Naumann, B.; Schweiger, S.; Hammel, J.; Müller, H.:

Parallel evolution of direct development in frogs - Skin and thyroid gland development in African Squeaker Frogs (Anura: Arthroleptidae: Arthroleptis).

In: Developmental Dynamics. Vol. 250 (2021) 4, 584 - 600.

First published online by Wiley: 22.12.2020

<https://dx.doi.org/10.1002/dvdy.275>

1 **Parallel evolution of direct development in frogs – Skin and thyroid gland development in**
2 **African Squeaker Frogs (Anura: Arthroleptidae: *Arthroleptis*)**

3

4 Benjamin Naumann^{1,*}, Susan Schweiger¹, Jörg U. Hammel², Hendrik Müller^{1,3,4,*}

5

6 ¹Institut für Zoologie und Evolutionsforschung, Erbertstraße 1, 07743 Jena, Germany

7 ²Helmholtz-Zentrum Geesthacht, Zentrum für Material- und Küstenforschung, Außenstelle am
8 DESY, Gebäude 66, Notkestraße 66, 22607 Hamburg, Germany

9 ³Zentralmagazin Naturwissenschaftlicher Sammlungen, Martin-Luther-Universität Halle-
10 Wittenberg, Domplatz 4, 06108 Halle (Saale), Germany

11 ⁴Department of Life Sciences, The Natural History Museum, Cromwell Road, London SW7
12 5BD, United Kingdom

13

14 *corresponding author: benjamin.naumann@uni-jena.de; hendrik.mueller@zns.uni-halle.de

15

16 Key words: *Cardioglossa*, tadpole, terrestrialization, heterochrony, developmental constraints

17

18

19

20 **Abstract**

21 Cases of parallel evolution offer the possibility to identify adaptive traits and to uncover
22 developmental constraints on the evolutionary trajectories of these traits. The independent
23 evolution of direct development, from the ancestral biphasic life history in frogs is such a case of
24 parallel evolution. In frogs, aquatic larvae (tadpoles) differ profoundly from their adult forms and
25 exhibit a stunning diversity regarding their habitats, morphology and feeding behaviors. The
26 transition from the tadpole to the adult is a climactic, thyroid hormone (TH)-dependent process of
27 profound and fast morphological rearrangement called metamorphosis. One of the organ systems
28 that experiences the most comprehensive metamorphic rearrangements is the skin. Direct-
29 developing frogs lack a free-swimming tadpole and hatch from terrestrial eggs as fully formed
30 froglets. In the few species examined, development is characterized by the condensed and
31 transient formation of some tadpole-specific features and the early formation of adult-specific
32 features during a “cryptic” metamorphosis. In this study we show that skin in direct-developing
33 African squeaker frogs (*Arthroleptis*) is also repatterned from a tadpole-like to an adult-like
34 histology during a cryptic metamorphosis. This repatterning correlates with an increase of thyroid
35 gland activity. A comparison with data from the Puerto Rican coqui (*Eleutherodactylus coqui*)
36 reveals that direct development might have evolved in parallel in these frogs by a comparable
37 heterochronic shift of thyroid gland activity. This suggests that the development of many adult-
38 features is still constrained by the ancestral dependency on thyroid hormone signaling.

39

40 **Introduction**

41
42 How do developmental constraints influence phenotypic evolution? A promising way to approach
43 this question is studying cases of parallel evolution (Schluter, Clifford, Nemethy, & McKinnon,
44 2004). Parallel evolution can be defined as the independent origin of similar (derived) traits in
45 two or more taxa sharing a common ancestry and bauplan (Futuyma & Kirkpatrick, 2017;
46 Simpson, 1961). Investigating patterns of parallel evolution allows to identify adaptive traits and
47 to uncover developmental constraints on the evolutionary trajectories of these traits (Schluter et
48 al., 2004). A potential case of parallel evolution is the repeated, independent origin of direct
49 development within frogs and other amphibians (San Mauro et al., 2014; Schweiger, Naumann,
50 Larson, Möckel, & Müller, 2017; Thibaudeau & Altig, 1999; Wake & Hanken, 1996). Direct
51 development is characterized by the loss of an aquatic larval phase (Hall & Olson, 2003) and may
52 have evolved in response to environmental conditions that restricted the availability of suitable
53 habitats for aquatic development (Goin & Goin, 1962; Liedtke et al., 2017; Müller et al., 2013;
54 ten Brink, Onstein, & de Roos, 2020).

55 In frogs, direct development evolved several times independently (Figure 1A), making them a
56 suitable model system to unravel developmental constraints that underlay patterns of parallel
57 evolution (Goldberg, Candiotti, & Akmentins, 2012; Heinicke et al., 2009). The ancestral biphasic
58 life history of frogs includes a free-swimming larval stage called tadpole (McDiarmid & Altig,
59 1999). In contrast to other amphibian larvae, tadpoles differ extremely from their adult forms and
60 exhibit a stunning diversity regarding their habitats, morphology and feeding behaviors (Altig &
61 McDiarmid, 1999). In biphasic anurans, embryonic development from a fertilized egg to a
62 tadpole happens more or less gradually, similar to other vertebrate groups. In contrast, the

63 transition from the tadpole to the adult is a climactic, thyroid hormone (TH)-dependent process of
64 profound and fast morphological rearrangement called metamorphosis (Shi, 1999) (Figure 1B). In
65 direct developing species, development from the embryo to the adult frog appears more gradual
66 without an obvious climactic phase (Callery, Fang, & Elinson, 2001) (Figure 1B). Tadpole-
67 specific traits such as the larval skeleton and its associated musculature, the cement glands, the
68 lateral line system and the coiled intestine are nearly or completely reduced (Callery et al., 2001;
69 Hanken, Klymkowsky, Alley, & Jennings, 1997). However, morphological studies on the
70 embryonic development of direct developing frogs are limited to only a few species (Goldberg et
71 al., 2012; Goldberg, Taucce, Quinzio, Haddad, & Candiotti, 2020; Hanken, Klymkowsky,
72 Summers, Seufert, & Ingebrigtsen, 1992; Kerney, Meegaskumbura, Manamendra-Arachchi, &
73 Hanken, 2007; Schweiger et al., 2017). The only species in which direct development has been
74 investigated in greater detail is the Puerto Rican coqui, *Eleutherodactylus coqui* Thomas, 1966
75 (thyroid gland: Laslo, Denver, & Hanken, 2019; Callery & Elinson, 2000; Elinson & Fang, 1998;
76 Jennings & Hanken, 1998; Fang & Elinson, 1996; limb development: Hanken et al., 2001; cranial
77 development: Hanken et al., 1997; Kerney, Gross, & Hanken, 2010; Olsson, Moury, Carl,
78 Håstad, & Hanken, 2002; Schlosser, Kintner, & Northcutt, 1999; Schlosser & Roth, 1997; gross
79 embryonic development: Townsend & Stewart, 1985).

80 Although direct-developing frogs have departed profoundly from their ancestral ontogeny
81 (Hanken et al., 1997; Schlosser, 2008; Schweiger et al., 2017), studies in *E. coqui* have shown
82 that several developmental events are still under the control of TH (Callery & Elinson, 2000;
83 Hanken & Summers, 1988) and that it undergoes a cryptic metamorphosis (Callery & Elinson,
84 2000; Ziermann & Diogo, 2014). The ontogenetic repatterning seen in direct-developing frogs is
85 thought to be the result of changes in the expression of TH, which leads to changes in timing of
86 TH-dependent events during development (“heterochronic shift” hypothesis). At least some

87 developmental events are thought to have become decoupled from TH-regulation (“loss of
88 constraint” hypothesis), but so far data are only available for *E. coqui* and the general influence
89 of TH during the ontogeny of other direct-developing frogs remains unclear.

90 An interesting system to study putative developmental constraints on the evolution of direct
91 development is the skin. The frog skin hosts a complex microbiome and plays major roles in
92 immune response, pathogen defense, respiration, osmoregulation, camouflage and even
93 reproduction (Douglas, Hug, & Katzenback, 2020; Fernandes et al., 2011; Huang et al., 2016;
94 Katz, 1986; Varga, Bui-Marinos, & Katzenback, 2019). Among all tissues that remodel during
95 metamorphosis the skin exhibits the most extreme changes regarding histology and gene
96 expression (Yoshizato, 1992). It is exposed to completely different environments (aquatic vs.
97 terrestrial) depending on life history phases and often exhibits tadpole- and adult-specific
98 adaptations (Quinzio & Goldberg, 2019). The skin of pre-metamorphic tadpoles is a mostly two-
99 layered epithelium with unicellular glands and an outer mucus layer (Duellman & Trueb, 1994).
100 The underlying dermis consists of a stratum compactum and some melanophores in the
101 mesenchyme beneath (Figure 1C). During pro-metamorphosis, the cells of the epidermis
102 degenerate except for cells attached to the basal lamina. These basal cells start to proliferate
103 during metamorphic climax and build up the post-metamorphic five- to seven-layered adult frog
104 epidermis with an outer keratinized cell layer (stratum corneum) and different multicellular gland
105 types. The underlying dermis contains an outer (exterior to the stratum compactum) and an inner
106 (interior to the stratum compactum) melanophore layer (Figure 1C) (Fox, 1985; Kinoshita &
107 Sasaki, 1994; Tamakoshi, Oofusa, & Yoshizato, 1998). Metamorphic changes in biphasic species
108 are initiated by thyroid hormone (TH) production (Brown & Cai, 2007; Kulkarni, Singamsetty, &
109 Buchholz, 2010; Tata, 2006). Thyroid hormone is also involved in several developmental

110 processes in *E. coqui* indicating the presence of a cryptic metamorphosis in direct developing
111 species (Callery & Elinson, 2000; Hanken et al., 1992; Kulkarni et al., 2010; Schlosser, 2008).

112 In this study, we provide detailed data on skin development in direct developing African
113 Squeaker frogs (*Arthroleptis*) using histological and immuno-histochemical techniques. To
114 evaluate if potential changes in the skin and thyroid gland histology of *Arthroleptis* are due to
115 direct development or instead shared by biphasic Arthroleptidae, we investigated the same tissues
116 in a *Cardioglossa* tadpole, the sister genus of *Arthroleptis*. Additionally, we describe thyroid
117 gland development in *Arthroleptis* and infer its activity based on morphology and morphometric
118 measurements.

119

120 **Results**

121 Many aspects of the development of the embryonic pigmentation pattern, skin and thyroid glands
122 are similar in *A. wahlbergii* and *A. xenodactyloides*. Differences between the two species are
123 mentioned where present.

124

125 **Development of the pigmentation pattern in *Arthroleptis* embryos**

126 Embryos until mid TS5 lack any obvious, externally visible pigmentation and have a white-
127 yellowish color (Figure 2A; see also Schweiger et al., 2017). However, very few melanophores
128 were found in the epidermal layer in histological sections of an embryo at TS4 (see Figure 3A4).
129 At late TS5/early TS6 melanophores are recognizable extending dorso-ventrad until the ventral
130 border of the eye in the head region and until the dorsal-most quarter of the lateral body wall in

131 the trunk region (Figure 2B). Melanophores at this stage are spindle-shaped with long, thin
132 extensions (Figure 2B`). From late TS7 to TS8, melanophores continue to extend ventrad in the
133 head and the trunk regions (Figure 2C, D) until they completely cover the lateral body wall from
134 TS9 on (Figure 2E, F). At this stage, the body wall has completely enclosed the yolk (Figure
135 2E3). At TS11, the density of melanocytes of the head region starts to increase resulting in a
136 darkening of the skin (Figure 2G). Additionally, another type of melanophores becomes visible
137 all over the body. These melanophores are smaller, with a more spherical shape and with only a
138 few short or no extensions (Figure 2G`). At TS12, melanocyte density continues to increase
139 dorso-ventrad until the whole lateral body wall is heavily pigmented at TS15 (Figure 2H-K).

140 In summary, pigmentation development is characterized by a first dorso-ventrad wave of
141 melanophore development starting at late TS5 and a second wave made up by a morphologically
142 different type of melanophores starting at TS11.

143

144 **Skin development in *Arthroleptis***

145 TS4 (Figure 3A) – The epidermis is single-layered with a sometimes indistinct border between
146 the underlying cells and tissues. In the dorsal body region, cells are large and cuboid with
147 spherical nuclei. Ventrally, cells are flattened and nuclei are ovoid to spindle-shaped. The cells
148 possess high amounts of intracellular yolk granules and some seem to have large vacuoles with
149 dark pigments. Ciliated cells are found in a scattered pattern all over the embryo. Very few
150 melanophores can be found intercalating between epidermal cells. A dense, undifferentiated
151 mesenchyme lies beneath the epidermis.

152 TS5 (Figure 3B) – The dorsal epidermis of the head as well as of the dorso-lateral trunk is two-
153 layered while the ventral epidermis of the trunk, covering the yolk sac, is single-layered. Most
154 cells are slightly flattened with ovoid nuclei. The amount of intracellular yolk granules has
155 decreased compared to TS4 but is still high. The number of ciliated cells has increased compared
156 to TS4. A sharp border between epidermal cells and the underlying mesenchyme is recognizable.

157 TS6 and TS7 (Figure 3C, D) – The number of epidermal layers has not changed compared to
158 TS5. Some unicellular mucus glands are recognizable. The amount of intracellular yolk granules
159 has further decreased compared to previous stages. A higher number of melanophores with long
160 cytoplasmic extensions are present in the mesenchyme directly beneath the epidermis.

161 TS8 (Figure 3E) – The number of epithelial layers is similar to previous stages. Epidermal cells
162 in both layers are flattened and show spindle-shaped nuclei. Some hypertrophied cells with a
163 granular content that might represent unicellular glands are present in the skin of the head.
164 Intracellular yolk granules are only detectable in the trunk epidermis. In the head, a distinct
165 stratum compactum is present beneath the epidermis with a dense layer of inner melanophores
166 interior to it. In the trunk, the stratum compactum is most distinct in the dorsal region and
167 becomes gradually less obvious in lateral and ventral areas. This pattern is mirrored by the
168 density of associated inner melanophores.

169 TS11 (Figure 3F) –The epidermis has become single-layered again in the head and dorsolateral
170 trunk region and epidermal cells exhibit extremely flattened nuclei. In some scattered areas of the
171 dorsal head, the epidermis is still two-layered. Intracellular yolk granules and ciliated cells are
172 completely absent. Multicellular gland primordia, consisting of several compact cells, can be
173 found all over the body. In the head, a few outer melanocytes are present between the stratum
174 compactum and basal epidermal cells. In the trunk, the stratum compactum appears denser

175 compared to the previous stage and the density of inner melanophores has increased. It is still
176 lowest in the ventral trunk region.

177 TS13 (Figure 3G) – The skin exhibits many features of an adult frog skin. The epidermis is two -
178 to three-layered. The majority of the basal epidermal cells are cuboid. The apical cell layer is
179 flattened and is stained dark-blue in Azan-stained section, indicating an increased keratinization
180 and the presence of a stratum corneum. The stratum corneum is more obvious in the head
181 compared to the trunk epidermis. Multicellular mucus and granular glands can be found in
182 various regions of the body. They are localized within a thin stratum spongiosum beneath the
183 basal epidermal cell layer. Mucus glands are outlined by a single cell layer with an inner lumen.
184 Granular glands are recognizable as large sacs filled with many granulated cells. The density of
185 outer melanophores within the now developed stratum spongiosum has increased compared to
186 previous stages.

187 TS15 (Figure 3H) – Hatching occurs at this stage and the skin of the froglet is similar to the skin
188 of an adult *Arthroleptis* (Supplementary material 2). The thickness of the epidermis varies from
189 two - to five cell layers but is three-layered in most areas. In the trunk region, the dark blue-
190 stained stratum corneum is now also recognizable as a distinct cellular layer. Multicellular glands
191 in the whole skin are more numerous and melanophore density has increased in the ventral trunk
192 region compared to TS13.

193 In summary, the embryonic ectoderm and underlying mesenchyme at TS4 differentiated into a
194 skin consisting of an epidermis and an underlying dermis both exhibiting pre-metamorphic
195 tadpole-typical features at TS8. At TS11 the apical epidermal layers seem to degenerate to a
196 certain degree while multicellular gland progenitors appear all over the body. The skin of
197 embryos at TS13 and TS15 exhibit many features typical for the post-metamorphic frog skin.

198

199 **PCNA expression during epidermal development in *Arthroleptis***

200 Metamorphic skin remodeling is based on the degeneration of apical epidermal cells and the
201 proliferation of remaining basal cells building the adult epidermis (Yoshizato, 1992). We
202 therefore investigated the epidermal proliferation pattern in embryonic stages of *A. wahlbergii*
203 using two different antibodies against proliferating cell nuclear antigen (PCNA). Signals from
204 both antibodies were detected in the same tissues of two adjacent serial sections verifying
205 antibody specificity. However, the signal from PCNA-1 antibody was always stronger than from
206 the PCNA-2 antibody.

207 At TS8, scattered signals of the PCNA-1 antibody are detectable in nuclei of both, epidermal cell
208 layers as well as some mesenchymal cells (Figure 4A, A'). Only a few PCNA-2 positive cells are
209 detectable at this stage (Figure 4B, B'). At TS11, PCNA-1 and PCNA-2 signals are detectable in
210 the majority of epidermal cells, indicating a strong increase in the proliferation rate of the
211 epidermis (Figure 4C, D). A few PCNA-1 and PCNA-2 positive mesenchymal cells are also
212 present. No antibody signals are detectable in the epidermis at TS13 and TS15, indicating a low
213 proliferation rate (Figure 4E-G). In some multicellular glands however, PCNA-1 positive cells
214 can be detected (Figure 4G).

215 In summary, PCNA reactivity (and therefore cell proliferation rate) of the skin is detectable in a
216 scattered pattern at TS8, has increased tremendously at TS11 and is low or absent at TS 13 and
217 TS15.

218

219 **Thyroid gland development in *Arthroleptis* embryos**

220 The thyroid glands are paired, ovoid structures located at the lateral edges of the hyoid plate
221 (Figure 5A-C). Primordia are first detectable at TS8. They appear as spherical, condensed cell
222 masses including scattered lumina which lack an epithelial lining. The primordia are located on
223 the left and right side ventrally to the lateral edges of the developing hyoid plate (Figure 5A, D).
224 First developing follicles are recognizable at TS10/11. The cells of the follicular epithelial are
225 cuboid with little cytoplasm and large spherical nuclei (Figure 5E). At later TS11, thyroid glands
226 have elongated, adopting a mature, adult-like morphology (Figure 5B). The follicles have
227 increased in size and number and the follicular epithelium is now organized in a columnar-
228 pattern. Nuclei of follicular epithelial cells are spherical to ovoid-shaped. Some colloid,
229 recognizable as a bluish substance in Azan-stained sections, is present within follicular lumina
230 (Figure 5F). At TS13 the follicles have further increased in size and number. The cells of the
231 follicular epithelium appear slightly flattened compared to the previous stage. No colloid is
232 detectable in the investigated specimen (Figure 5G). At TS15 the thyroid glands have continued
233 to elongate and are almost spindle-shaped (Figure 5C). The size and number of follicles have
234 further increased and the follicular lumina are filled with colloid in the investigated specimen.
235 Erythrocytes are recognizable around and in between follicles indicating a continuous
236 vascularization of the thyroid gland (Figure 5H).

237 We therefore measured the cell height of the follicular epithelium as well as the number and
238 diameter of follicles (Figure 6B-D). All measurements were taken from sections from the central
239 region of the thyroid gland (Cruz & Fabrezi, 2020). In *A. wahlbergi* we observed a huge increase
240 in the follicle cell height from TS8 to TS10/11, followed by a gradual decrease in TS 13 and
241 TS15. In the two examined stages of *A. xenodactyloides* cells were smaller compared to *A.*

242 *wahlbergii*. However, a similar but lower decrease in cell height from TS11 to TS15 is also
243 recognizable (Figure 6B). Follicle numbers and follicle number are more or less similar in *A.*
244 *wahlbergii* and *A. xenodactyloides* (Figure 6C, D). In *A. wahlbergi*, follicle number and diameter
245 decrease from TS8 to TS10/11 and then increases gradually from TS10/11 to TS15. In the two
246 specimens of *A. xenodactyloides*, an increase in follicle number and diameter can also be
247 observed.

248 In summary, our data indicate that thyroid glands differentiate histologically between TS8 and
249 TS10/11, become highly active at TS11 (follicle cell height, first detected colloid) and develop
250 and adult-like morphology between TS 13 and TS15 (increasing follicle diameter and number,
251 decreasing cell height).

252

253 **Skin and thyroid gland histology in a *Cardioglossa* tadpole**

254 The skin of *Cardioglossa* sp. at Gosner-stage 27 (Gosner, 1960) exhibits a pattern typical for the
255 majority of tadpoles (McDiarmid & Altig, 1999). The epidermis is two-layered. The basal layer
256 consists of cuboid cells with spherical nuclei while the apical layer is slightly flattened in the
257 head but not in the trunk region (Figure 7A1-A5). A dark-blue stained extracellular layer
258 resembling the keratinized apical cell layer present in late *Arthroleptis* embryos can be found.
259 Some unicellular gland cells are present in between basal and apical cells (Figure 7A1, A3). A
260 thick stratum compactum is present beneath the basal epidermal layer. Melanophores are
261 associated with the stratum compactum. Their density decreases dorso-ventrad in the head as well
262 as the trunk region (Figure 7A1-A5).

263 The thyroid glands exhibit a more elongated olive-shape and are localized in the same position as
264 described for *Arthroleptis* embryos (Figure 7B). At this developmental stage, well developed
265 follicle outlines by slightly flattened epithelial cells can be recognized. No colloid or
266 vascularization has been detected in the examined specimen. The flattened follicular epithelial
267 cells and the absence of colloid and vascularization indicate a low activity of TH-production.

268

269 **Discussion**

270

271 ***Arthroleptis* exhibits accelerated body wall fusion and a phase of metamorphic skin** 272 **pigmentation repatterning that correlates with increased thyroid gland activity**

273 The skin of frogs harbors a variety of chromatophores (Duellman & Trueb, 1994). In this study
274 however we focus on the pattern of melanophores only. Different types of melanophores are
275 present in the adult frog skin (Yasutomi, 1987). This adult pigmentation pattern is established via
276 metamorphic changes in the dermal pigmentation, chromophore morphology, and biochemistry
277 of the tadpole skin (Yasutomi, 1987). This indicates a correlation of TH production and
278 metamorphic skin pigmentation repatterning in biphasic anurans (Smith-Gill & Carver, 1981).

279 In direct developing species, pigmentation patterning has only been described in *E. coqui*
280 (Townsend and Stewart, 1985). At TS7, first melanophores appear in the trunk region and
281 pigmentation increases slowly until it becomes heavy at TS10. Pigmentation of the head is
282 delayed becoming heavy at TS12. This general process of melanophore patterning is also seen in
283 *Arthroleptis* (Schweiger et al., 2017; this study) and we here provide the first detailed data on the

284 morphology of different melanophore types during skin development in a direct developing frog
285 species. In *Arthroleptis*, the first type of melanophore is spindle-shaped with long thin extensions.
286 This type is typical of embryonic melanophores in biphasic species (Smith-Gill & Carver, 1981;
287 Yasutomi, 1987). A second type of melanophore with a smaller, more circular-shape with a few
288 short or no extensions appears at around TS11. This melanophore type resembles melanophores
289 appearing during TH-mediated metamorphosis in biphasic species (Smith-Gill & Carver, 1981;
290 Yasutomi, 1987). It is generally accepted that follicular cell height, follicle diameter and number
291 (see Figure 6A) roughly reflect thyroid gland activity and TH production (Coleman, Evennett, &
292 Dodd, 1968; Grim et al., 2009). Therefore, the appearance of this second melanophore type
293 correlates with an increased thyroid activity. The timing of pigmentation repatterning and
294 melanophore type appearance in *Arthroleptis* is very similar to the TH-mediated metamorphic
295 transitions seen in the skin of biphasic species (Smith-Gill & Carver, 1981; Yasutomi, 1987).

296 Experimental studies on the pigmentation pattern (Elinson & Fang, 1998) and histological
297 investigation of thyroid gland activity (Jennings & Hanken, 1998) in *E. coqui* led to the
298 suggestion that TH is also involved in the closure of the pigmented body surface (Callery &
299 Elinson, 2000; Elinson & Fang, 1998). While the overall melanophore patterning and subsequent
300 darkening of the skin are similar in *Arthroleptis* and *E. coqui*, there is a difference in the timing
301 of the ventral fusion of the pigmented lateral body walls

302 This fusion appears much earlier in *Arthroleptis* (TS9, Figure 2) compared to *E. coqui* (TS12,
303 Elinson & Fang, 1998). In *E. coqui* this event correlates with a peak in thyroid gland activity
304 (Laslo et al., 2019) and has experimentally shown to be TH dependent (Callery & Elinson, 2000).
305 In *Arthroleptis*, histologically inferred thyroid activity peaks at TS10/11. Therefore fusion of the
306 lateral body walls seems slightly accelerated. This could be due to a higher TH-sensitivity of the

307 lateral body wall tissue or the earlier expression of TH that cannot be detected histologically.
308 Experimental and molecular/immuno-histochemical or mass spectroscopic data from *Arthroleptis*
309 are needed to clarify this.

310
311 **Skin histology in *Arthroleptis* exhibits a phase of metamorphic repatterning that correlates**
312 **with increased thyroid gland activity**

313
314 Skin and thyroid gland histology of the *Cardioglossa* tadpole are similar to many other tadpoles
315 at a comparable developmental stage (Cruz & Fabrezi, 2020). Alterations in skin development in
316 *Arthroleptis* therefore seem to be correlated with the evolution of direct development. However,
317 an apical extracellular layer resembling the stratum corneum in adult frog skin is present in the *C.*
318 *manengouba* tadpole. Tadpoles of various species of *Cardioglossa*, including *C. manengouba*,
319 have been frequently found buried in sediment and other substrate in streams (Blackburn, 2008;
320 Hirschfeld, Barej, Gonwouo, & Rödel, 2012) and this putative stratum corneum could be an
321 adaptation to their fossorial life style.

322 As reported for *E. coqui* (Fang & Elinson, 1996; Schlosser et al., 1999), major tadpole characters
323 such as cement glands, neuromasts and skein cells (Tamakoshi et al., 1998) were not observed in
324 *Arthroleptis*. Data for *I. henselii* are not available (Goldberg et al., 2020). In *Arthroleptis*, skin
325 development can be divided into four major phases (embryonic, “tadpole”, metamorphic and
326 adult; Figure 8) that are also typical for many biphasic species (Fox, 1986; Robinson &
327 Heintzelman, 1987). At TS4 embryonic ectoderm is a single-cell layered epithelium not yet
328 differentiated into an epidermis. At around TS7 the ectodermal cells have differentiated into a
329 tadpole-like epidermis (two-layered, unicellular glands, inner melanophores). However, the

330 epidermis still exhibits some embryonic features (intracellular yolk granules, low melanophore
331 density, ciliated cells and the lack of a stratum compactum; Figure 8). At TS8, the skin exhibits
332 more mature tadpole-like features such as fewer intracellular yolk granules and ciliated cells, a
333 higher melanophore density, many unicellular glands and a stratum compactum. At TS11,
334 degeneration of the apical epidermal layer and unicellular glands together with the appearance of
335 multicellular gland progenitors and an additional outer melanophore layer (Figure 8) resembles
336 skin repatterning during the metamorphic climax of biphasic species (Fox, 1985; Gaupp, 1904;
337 Verma, 1965). In biphasic species, shortly before metamorphic climax, apical cells in the tadpole
338 epidermis undergo apoptosis except for the single layer of basal cells. The remaining basal cells
339 proliferate extensively during metamorphic climax building up the adult epidermis and gland
340 cells (Kinoshita & Sasaki, 1994; Schreiber & Brown, 2003; Yoshizato, 1992). In *Arthroleptis*,
341 metamorphic skin repatterning is seen at TS11, when the “tadpole” apical epidermal layer
342 degenerates and cells in the remaining basal layer start to proliferate (Figure 8; strong PCNA
343 signal). This patterning of the tadpole-like skin and increased PCNA activity correlate with an
344 increase of histologically inferred thyroid gland activity at TS10/11 (see Figure 6). From TS13
345 on, the skin of *Arthroleptis* exhibits major features of an adult frog skin, such as a multilayered
346 (three to five layers dorsally) epidermis with an apical stratum corneum, large multicellular
347 glands embedded into a stratum spongiosum and a layer of outer and inner melanophores
348 bordering the thick stratum compactum (Figure 8). This in term correlates with a decreased
349 thyroid gland activity and the absence of a PCNA signal in epidermal cells.

350 Regarding other direct developing species, detailed histological data are only available for two
351 developmental stages of *Ischnocnema henselii* (Goldberg et al., 2020). At TS6, the epidermis of
352 this species is a single-layered epithelium overlaying an undifferentiated mesenchymal dermis
353 (Goldberg et al., 2020). This is very similar to *Arthroleptis* embryos except that the epidermis is

354 two-layered in most body regions at this developmental stage. In *I. henselii* embryos at TS14,
355 epidermal cells start to proliferate forming a two-layered epidermis. Ciliated cells are still present
356 in many body areas, progenitors of multicellular glands are detectable and melanocyte density
357 has increased compared to TS6. The dermis has also differentiated and a stratum compactum is
358 present (Goldberg et al., 2020). This is different to *Arthroleptis*, where the features described for
359 *I. henselii* at TS14 are already present at TS11 (Figure 8). In contrast to *I. henselii*, the short
360 description of a stage likely corresponding to TS9 in *Eleutherodactylus* that exhibits a two-
361 layered epidermis (Adamson, Harrison, & Bayley, 1960), implies an earlier pattern of skin
362 differentiation more similar to *Arthroleptis*. This is very interesting since a differentiated thyroid
363 gland is already present at TS6 in *I. henselii*. This is much earlier compared to *Arthroleptis* (TS8;
364 this study) and *E. coqui* (TS10; Jennings & Hanken, 1998) and skin development does therefore
365 not seem to correlate with thyroid gland maturation in *I. henselii*.

366 This mismatch between very early TH gland maturation and very late skin remodeling in *I.*
367 *henselli* could be indicative of a loss of TH-dependency of skin remodeling and hence a loss of
368 constraint. Alternatively, skin maturation might still be dependent on TH-signaling, but TH-
369 production of the thyroid gland could be very low and a concentration necessary to induce skin
370 repatterning is reached very late. Another possibility is that TH-levels are normal but the
371 sensitivity of the skin tissue is decreased, requiring higher TH concentrations to induce
372 repatterning. Both of these TH-dependent scenarios would explain the late onset (i.e.
373 heterochronic shift) of skin remodeling.

374

375 **Thyroid gland development and activity in direct developing frogs**

376 As it has been shown that metamorphic changes in anurans, and amphibians in general, are under
377 a complex hormonal control but TH seems to be a major regulator (Shi, 1999). There are two
378 hypotheses how the ancestral thyroid axis has influenced the evolution of direct development (see
379 Jennings & Hanken, 1998 and references therein). (1) Thyroid gland activity and TH production
380 are activated early in development leading to a precocious formation of adult features. Direct
381 development is constrained by the ancestral dependency on TH for adult development.
382 Consequently, direct development evolved by a heterochronic shift (Gould, 1977) of ancestral
383 developmental mechanisms rather than the loss of constraints from it (“heterochronic shift”
384 hypothesis). (2) Metamorphosing tissues lost their ancestral TH-dependency. In this case, the loss
385 of constraints would have been more important in the evolution of direct development than
386 heterochronic shifts of ancestral mechanisms (“loss of constraint” hypothesis).

387 Experimental studies on *E. coqui* have shown that this species exhibits a mosaic pattern of
388 heterochronic shifts and loss of constraints for different morphological features (Callery &
389 Elinson, 2000; Hanken et al., 1997; Hughes, 1966; Hughes & Reier, 1972; Jennings & Hanken,
390 1998; Lynn, 1948; Lynn & Peadon, 1955; Townsend & Stewart, 1985).

391 There are many similarities between *E. coqui* and *Arthroleptis* regarding metamorphic
392 repatterning processes that correlate with increased thyroid activity such as tail regression,
393 remodeling of the “larval” into the adult hyobranchial apparatus and cranial muscle repatterning,
394 (Hanken et al., 1997; Jennings & Hanken, 1998; Schweiger et al., 2017; Schweiger, Naumann, &
395 Müller, in prep.; Townsend & Stewart, 1985). Most of these processes start slightly earlier in
396 *Arthroleptis*, which correlates with an earlier appearance of the thyroid glands compared to *E.*
397 *coqui* (Hanken & Jennings, 1998; this study). *Ischnocnema henselii* might be another example

398 where some features of skin development might have lost their dependency on TH, but the
399 interpretation of the data for *I. henselii* is hampered by the lack of a detailed investigation of
400 thyroid gland and skin development over several developmental stages.

401 However, our data indicate that many tadpole specific structures appear, differentiate and are
402 repatterned to the adult configuration during a short metamorphic phase although this cryptic
403 metamorphosis appears to be not as climactic as in biphasic frogs.

404

405 **Developmental constraints, heterochrony and the parallel evolution of direct development**

406 Direct development has evolved parallel in different groups of frogs. The comparison of
407 embryonic development of these direct developing frogs offers the possibility to identify how
408 developmental constraints may have influenced the observed pattern of parallel evolution. Many
409 developmental mechanisms are governed by major regulators such as TH. In case of a
410 heterochronic shift of this regulator (e.g. embryonic thyroid activity in direct developing frogs),
411 traits that are under the control of this regulator have to follow this shift. These traits are
412 constrained by this major regulator. Other traits that do not follow the heterochronic shift of this
413 regulator develop normally and are not constrained. This may lead to a decoupling of ancestrally
414 synchronous processes such as, e.g., growth and differentiation of the retinotectal system in *E.*
415 *coqui* (Schlosser, 2008).

416 Further investigations of the developmental timing and TH-dependency of anatomical features of
417 *Eleutherodactylus*, *Arthroleptis*, *Ischnocnema* and other direct developing frogs are needed.
418 These investigations will clarify if homologous features are generally under the control of TH
419 and therefore constrained by thyroid gland activity. Studies on direct development in frogs, or

420 amphibians in general, and various other cases such as the classic example of the evolution of
421 similar morphotypes in African cichlids (Elmer et al., 2014; Meier, Marques, Wagner, Excoffier,
422 & Seehausen, 2018) or the recently “re-discovered” dispersion/re-aggregation and diapause
423 phases in early killifish development (Furness, Reznick, Springer, & Meredith, 2015; Naumann
424 & Englert, 2018) will help to better understand how developmental processes constrain the
425 evolution of adaptive traits and to further clarify mechanisms and identifying major regulators
426 underlying parallel evolution.

427

428 **Experimental Procedures**

429 **Specimens**

430 Embryos of *Arthroleptis wahlbergii* Smith, 1849, collected in South Africa, and *A.*
431 *xenodactyloides* Hewitt, 1933, collected in Tanzania, were euthanized using 0.1 % tricaine
432 methanesulfonate (MS222, Fluka), fixed in 4% phosphate buffered formalin and stored in 70%
433 ethanol (Schweiger et al., 2017). Staging of embryos follows Townsend and Stewart (1985); TS
434 stages hereafter. One tadpole of *Cardioglossa manengouba* Blackburn, 2008 was available for
435 investigation. For a complete list of specimen see Supplementary material 1.

436

437 **Histological sectioning and staining**

438 For sectioning, embryos were dehydrated in an ethanol series (70%, 90%, 2 x 96%; 5 min each),
439 sectioned and subsequently rehydrated (2 x 96%, 90%, 70% ethanol, distilled water; 5 min each)
440 prior to staining. Embryos up to TS8 were embedded in Technovit 8100 (Kulzer, R0010022),
441 sectioned at 3 μ m and stained with a mixture of basophilic Methylene blue and acidic Fuchsin

442 (Mulisch & Welsch, 2010). Embryos from TS10/11 on were decalcified for up to three days
443 (Osteomoll, Merck), embedded in Paraplast (Roth, X881.1), sectioned at 8 μm and stained with
444 Heidenhain's Azan (Mulisch & Welsch, 2010). All sections were made using a Microm HM 360
445 (Zeiss) and photographs were taken using an Olympus Dotslide BX51 microscope.

446

447 **Fluorescent antibody staining**

448 Paraffin sections were rehydrated as described before. For antigen retrieval, slides were
449 transferred to a plastic cuvette with citrate buffer (recipe see Schlosser, 2008) and heated in a
450 microwave (Bosch HMT 72M 420) for 10 minutes at 180W. Subsequently, slides were placed at
451 room temperature (RT, 21-25°C) to cool down for at least 5 minutes and then rinsed in distilled
452 water for 1 minute. Afterwards, slides were rinsed with PBS (3 x 5 minutes), placed into a wet
453 chamber and blocked with antibody diluent (DAKO) for 1 hour at RT. Primary antibodies against
454 proliferating cell nuclear antigen (PCNA-1, 1/200, sc-7907, Santa Cruz; PCNA-2, 1/200,
455 M087901, Dako) were applied overnight at 4°C. On the next day, slides were rinsed in PBS (3 x
456 5 minutes), blocked and incubated with secondary antibodies (Alexa-488 anti-mouse, #A28175,
457 Thermo Fisher Scientific and Alexa-568 anti-rabbit, #A-11011, Thermo Fisher Scientific) for 1
458 hour at RT. Afterwards, slides were rinsed with PBS (3 x 5 minutes), quickly washed with
459 distilled water and cover-slipped with Fluoroshield with DAPI (Sigma, F6057). Slides were
460 photographed using a Zeiss Axioplan Microscope equipped with a Spot camera and the Zeiss
461 Axioplan software.

462

463 **Micro-CT scanning and 3D reconstruction**

464 Specimens were contrasted using a solution of 1% polymolybdenic acid in 70% ethanol
465 (Metscher, 2009). *Arthroleptis* specimens were CT-scanned using a Nanotom S μ CT scanner
466 (Phoenix X-Ray) and the *Cardioglossa* tadpole was studied using synchrotron radiation based x-
467 ray micro-CT. Imaging was performed at the Imaging Beamline P05 (IBL) (Greving et al., 2014;
468 Haibel et al., 2010; Wilde et al., 2016) operated by the Helmholtz-Zentrum-Geesthacht at the
469 storage ring PETRA III (Deutsches Elektronen Synchrotron – DESY, Hamburg, Germany) using
470 a photon energy of 24 keV. Projections were recorded using a CCD camera system (MicroLine
471 ML09000 - Finger Lake Instruments) with an effective pixel size of 2.42 μ m. For each
472 tomographic scan 1801 projections at equal intervals between 0 and π have been recorded.
473 Tomographic reconstruction has been done by applying a filtered back projection algorithm
474 (FBP) implemented in a custom reconstruction pipeline (Moosmann et al., 2014) using Matlab
475 (Math-Works) and the Astra Toolbox (Palenstijn, Batenburg, & Sijbers, 2011; van Aarle et al.,
476 2016; van Aarle et al., 2015). For the tomographic reconstruction, raw projections were binned
477 two times resulting in an effective pixel size of the reconstructed volume of 4.83 μ m. Three-
478 dimensional reconstructions and mixed surface-volume renderings of the thyroid gland were
479 prepared using AMIRA 5.4.2 (FEI Visualization, Science Group, Bordeaux, France).

480

481 **Follicle cell height and follicle diameter measurements**

482 Qualitative and quantitative descriptions of thyroid glands are based on sections from the middle
483 region of the paired thyroid lobes according to Cruz and Fabrezi (2020). Measurements of follicle
484 cell heights and follicle diameter were obtained from digitalized sections using ImageJ
485 (Schneider, Rasband, & Eliceiri, 2012). A box and whisker plot of follicle cell heights was

486 prepared using Microsoft Excel 2010. Numbers of follicles were counted and mean values of the
487 measured follicle diameters were calculated for each specimen investigated.

488

489 **Photographs and Image processing**

490 Photographs of whole embryos were taken using a Zeiss Discovery V12 stereomicroscope with
491 an attached Zeiss AxioCam digital camera. Brightness and Contrast of Images was adjusted using
492 either ImageJ or Adobe Photoshop CS6. Channel colors of fluorescent antibody staining were
493 assigned in ImageJ. In some images the “CLAHE” filter implemented in ImageJ was applied to
494 enhance local contrast.

495

496 **Acknowledgements**

497 We would like to thank Katja Felbel for valuable help in the laboratory. We thank Mark-Oliver
498 Rödel for critical reading of the manuscript and a photograph of an adult *C. manengouba* and
499 Mareike Hirschfeld for a photograph of a *C. manengouba* tadpole. We thank Lennart Olsson for
500 critical reading of the manuscript. We thank Paul Lukas for help with the Dot Slide Microscope.
501 We would also like to thank Christoph Englert, Birgit Perner and Dagmar Kruspe for the kind gift
502 of the two PCNA antibodies.

503 **References**

- 504 Adamson, L., Harrison, R., & Bayley, I. (1960). *The development of the whistling frog*
505 *Eleutherodactylus martinicensis of Barbados*. Paper presented at the Proceedings of the
506 Zoological Society of London.
- 507 Altig, R., & McDiarmid, R. (1999). Diversity: familial and generic characterizations.

508 Blackburn, D. C. (2008). A new species of *Cardioglossa* (Amphibia: Anura: Arthroleptidae)
509 endemic to Mount Manengouba in the Republic of Cameroon, with an analysis of
510 morphological diversity in the genus. *Zoological Journal of the Linnean Society*, 154(3),
511 611-630.

512 Brown, D. D., & Cai, L. (2007). Amphibian metamorphosis. *Developmental Biology*, 306(1), 20.

513 Callery, E. M., & Elinson, R. P. (2000). Thyroid hormone-dependent metamorphosis in a direct
514 developing frog. *Proceedings of the National Academy of Sciences*, 97(6), 2615-2620.

515 Callery, E. M., Fang, H., & Elinson, R. P. (2001). Frogs without polliwogs: evolution of anuran
516 direct development. *BioEssays*, 23(3), 233-241.

517 Coleman, R., Evennett, P., & Dodd, J. (1968). Ultrastructural observations on the thyroid gland
518 of *Xenopus laevis* Daudin throughout metamorphosis. *General Comparative*
519 *Endocrinology*, 10(1), 34-46.

520 Cruz, J. C., & Fabrezi, M. (2020). Histology and microscopic anatomy of the thyroid gland
521 during the larval development of *Pseudis platensis* (Anura, Hylidae). *Journal of*
522 *Morphology*, 281(1), 122-134.

523 Douglas, A. J., Hug, L. A., & Katzenback, B. A. (2020). Composition of the North American
524 wood frog (*Rana sylvatica*) skin microbiome and seasonal variation in community
525 structure. *bioRxiv*.

526 Duellman, W. E., & Trueb, L. (1994). *Biology of Amphibians*: JHU press.

527 Elinson, R., & Fang, H. (1998). Secondary coverage of the yolk by the body wall in the direct
528 developing frog, *Eleutherodactylus coqui*: an unusual process for amphibian embryos.
529 *Development Genes and Evolution*, 208(8), 457-466.

530 Elmer, K. R., Fan, S., Kusche, H., Spreitzer, M. L., Kautt, A. F., Franchini, P., & Meyer, A.
531 (2014). Parallel evolution of Nicaraguan crater lake cichlid fishes via non-parallel routes.
532 *Nature Communications*, 5(1), 1-8.

533 Fang, H., & Elinson, R. P. (1996). Patterns of Distal-less gene expression and inductive
534 interactions in the head of the direct developing frog *Eleutherodactylus coqui*.
535 *Developmental Biology*, 179(1), 160-172.

536 Feng, Y.-J., Blackburn, D. C., Liang, D., Hillis, D. M., Wake, D. B., Cannatella, D. C., & Zhang,
537 P. (2017). Phylogenomics reveals rapid, simultaneous diversification of three major
538 clades of Gondwanan frogs at the Cretaceous–Paleogene boundary. *Proceedings of the*
539 *National Academy of Sciences*, 114(29), E5864-E5870.

540 Fernandes, T. L., Antoniazzi, M. M., Sasso-Cerri, E., Egami, M. I., Lima, C., Rodrigues, M. T.,
541 & Jared, C. (2011). Carrying progeny on the back: reproduction in the Brazilian aquatic
542 frog *Pipa carvalhoi*. *South American Journal of Herpetology*, 6(3), 161-176.

543 Fox, H. (1985). Changes in amphibian skin during larval development and metamorphosis. In M.
544 B. M Balls (Ed.), *Metamorphosis*: Clarendon Press, Oxford.

545 Fox, H. (1986). The skin of amphibia. *Biology of the Integument, Vertebrates*, 2, 78-148.

546 Furness, A. I., Reznick, D. N., Springer, M. S., & Meredith, R. W. (2015). Convergent evolution
547 of alternative developmental trajectories associated with diapause in African and South
548 American killifish. *Proceedings of the Royal Society B: Biological Sciences*, 282(1802),
549 20142189.

550 Futuyma, D., & Kirkpatrick, M. (2017). *Evolution*. Sinauer. Sunderland, MA.

551 Gaupp, E. (1904). *A. Ecker's und R. Wiedersheim's Anatomie des Frosches. Band 3. Lehre von*
552 *den Eingeweiden, dem Integument und den Sinnesorganen*: Vieweg.

553 Goin, O. B., & Goin, C. J. (1962). Amphibian eggs and the montane environment. *Evolution*,
554 364-371.

555 Goldberg, J., Candiotti, F. V., & Akmentins, M. S. (2012). Direct-developing frogs: ontogeny of
556 *Oreobates barituensis* (Anura: Terrarana) and the development of a novel trait. *Amphibia-*
557 *Reptilia*, 33(2), 239-250.

558 Goldberg, J., Taucce, P. P., Quinzio, S. I., Haddad, C. F., & Candiotti, F. V. (2020). Increasing
559 our knowledge on direct-developing frogs: The ontogeny of *Ischnocnema henselii*
560 (Anura: Brachycephalidae). *Zoologischer Anzeiger*, 284, 78-87.

561 Gosner, K. L. (1960). A simplified table for staging anuran embryos and larvae with notes on
562 identification. *Herpetologica*, 16(3), 183-190.

563 Gould, S. J. (1977). *Ontogeny and phylogeny*: Harvard University Press.

564 Greving, I., Wilde, F., Ogurreck, M., Herzen, J., Hammel, J. U., Hipp, A., . . . Beckmann, F.
565 (2014). *P05 imaging beamline at PETRA III: first results*. Paper presented at the
566 Proceedings of SPIE - Developments in X-Ray Tomography IX, San Diego, California,
567 United States.

568 Grim, K. C., Wolfe, M., Braunbeck, T., Iguchi, T., Ohta, Y., Tooi, O., . . . Tietge, J. (2009).
569 Thyroid histopathology assessments for the amphibian metamorphosis assay to detect
570 thyroid-active substances. *Toxicologic Pathology*, 37(4), 415-424.

- 571 Haibel, A., Ogurreck, M., Beckmann, F., Dose, T., Wilde, F., Herzen, J., . . . Mohr, J. (2010).
572 *Micro- and nano-tomography at the GKSS Imaging Beamline at PETRA III*. Paper
573 presented at the SPIE Optical Engineering + Applications.
- 574 Hall, B. K., & Olson, W. M. (2003). *Keywords and Concepts in Evolutionary Developmental*
575 *Biology*: Harvard University Press.
- 576 Hanken, J., Carl, T. F., Richardson, M. K., Olsson, L., Schlosser, G., Osabutey, C. K., &
577 Klymkowsky, M. W. (2001). Limb development in a “nonmodel” vertebrate, the
578 direct-developing frog *Eleutherodactylus coqui*. *Journal of Experimental Zoology*,
579 *291*(4), 375-388.
- 580 Hanken, J., Klymkowsky, M. W., Alley, K. E., & Jennings, D. H. (1997). Jaw muscle
581 development as evidence for embryonic repatterning in direct-developing frogs.
582 *Proceedings of the Royal Society B: Biological Sciences*, 1349-1354.
- 583 Hanken, J., Klymkowsky, M. W., Summers, C. H., Seufert, D. W., & Ingebrigtsen, N. (1992).
584 Cranial ontogeny in the direct-developing frog, *Eleutherodactylus coqui* (Anura:
585 Leptodactylidae), analyzed using whole-mount immunohistochemistry. *Journal of*
586 *Morphology*, *211*(1), 95-118.
- 587 Hanken, J., & Summers, C. H. (1988). Skull development during anuran metamorphosis: III.
588 Role of thyroid hormone in chondrogenesis. *Journal of Experimental Zoology*, *246*(2),
589 156-170.
- 590 Heinicke, M. P., Duellman, W. E., Trueb, L., Means, D. B., MacCulloch, R. D., & Hedges, S. B.
591 (2009). A new frog family (Anura: Terrarana) from South America and an expanded
592 direct-developing clade revealed by molecular phylogeny. *Zootaxa*, *2211*(1), 1-35.
- 593 Hewitt, J. (1933). Descriptions of some new reptiles and a frog from Rhodesia. *Occasional*
594 *Papers of the National Museum of Southern Rhodesia*, *2*, 45-50.
- 595 Hirschfeld, M., Barej, M. F., Gonwouo, N. L., & Rödel, M.-O. (2012). Tadpole descriptions of
596 three *Cardioglossa* species from southwestern Cameroon (Amphibia: Anura:
597 Arthroleptidae). *Salamandra*, *48*(3), 147-156.
- 598 Huang, L., Li, J., Anboukaria, H., Luo, Z., Zhao, M., & Wu, H. (2016). Comparative
599 transcriptome analyses of seven anurans reveal functions and adaptations of amphibian
600 skin. *Scientific reports*, *6*(1), 1-11.
- 601 Hughes, A. (1966). The thyroid and the development of the nervous system in *Eleutherodactylus*
602 *martinicensis*: an experimental study. *Development*, *16*(3), 401-430.

- 603 Hughes, A., & Reier, P. (1972). A preliminary study on the effects of bovine prolactin on
604 embryos of *Eleutherodactylus ricordii*. *General and Comparative Endocrinology*, 19(2),
605 304-312.
- 606 Jennings, D. H., & Hanken, J. (1998). Mechanistic basis of life history evolution in anuran
607 amphibians: thyroid gland development in the direct-developing frog, *Eleutherodactylus*
608 *coqui*. *General Comparative Endocrinology*, 111(2), 225-232.
- 609 Katz, U. (1986). The role of amphibian epidermis in osmoregulation and its adaptive response to
610 changing environment. In *Biology of the Integument* (pp. 472-498): Springer.
- 611 Kerney, R., Gross, J. B., & Hanken, J. (2010). Early cranial patterning in the direct-developing
612 frog *Eleutherodactylus coqui* revealed through gene expression. *Evolution &*
613 *Development*, 12(4), 373-382.
- 614 Kerney, R., Meegaskumbura, M., Manamendra-Arachchi, K., & Hanken, J. (2007). Cranial
615 ontogeny in *Philautus silus* (Anura: Ranidae: Rhacophorinae) reveals few similarities
616 with other direct-developing anurans. *Journal of Morphology*, 268(8), 715-725.
- 617 Kinoshita, T., & Sasaki, F. (1994). Body-specific proliferation of adult precursor cells in *Xenopus*
618 larval epidermis. *Histochemistry*, 101(6), 397-404.
- 619 Kulkarni, S. S., Singamsetty, S., & Buchholz, D. R. (2010). Corticotropin-releasing factor
620 regulates the development in the direct developing frog, *Eleutherodactylus coqui*. *General*
621 *and Comparative Endocrinology*, 169(3), 225-230.
- 622 Laslo, M., Denver, R. J., & Hanken, J. (2019). Evolutionary conservation of thyroid hormone
623 receptor and deiodinase expression dynamics in ovo in a direct-developing frog,
624 *Eleutherodactylus coqui*. *Frontiers in Endocrinology*, 10, 307.
- 625 Liedtke, H. C., Müller, H., Hafner, J., Penner, J., Gower, D. J., Mazuch, T., . . . Loader, S. P.
626 (2017). Terrestrial reproduction as an adaptation to steep terrain in African toads.
627 *Proceedings of the Royal Society B: Biological Sciences*, 284(1851), 20162598.
- 628 Lynn, W. G. (1948). The effects of thiourea and phenylthiourea upon the development of
629 *Eleutherodactylus ricordii*. *The Biological Bulletin*, 94(1), 1-15.
- 630 Lynn, W. G., & Peadon, A. M. (1955). The role of the thyroid gland in direct development in the
631 anuran, *Eleutherodactylus martinicensis*. *Growth*, 19(4), 263.
- 632 McDiarmid, R., & Altig, R. (1999). *Tadpoles: the Biology of Anuran Larvae*: University of
633 Chicago Press.

- 634 Meier, J. I., Marques, D. A., Wagner, C. E., Excoffier, L., & Seehausen, O. (2018). Genomics of
635 parallel ecological speciation in Lake Victoria cichlids. *Molecular Biology and Evolution*,
636 35(6), 1489-1506.
- 637 Metscher, B. D. (2009). MicroCT for comparative morphology: simple staining methods allow
638 high-contrast 3D imaging of diverse non-mineralized animal tissues. *BMC Physiology*,
639 9(1), 11.
- 640 Moosmann, J., Ershov, A., Weinhardt, V., Baumbach, T., Prasad, M. S., LaBonne, C., . . .
641 Hofmann, R. (2014). Time-lapse X-ray phase-contrast microtomography for in vivo
642 imaging and analysis of morphogenesis. *Nature Protocols*, 9(2), 294-304.
643 doi:10.1038/nprot.2014.033
- 644 Mulisch, M., & Welsch, U. (2010). *Romeis Mikroskopische Technik*: Spektrum Akademischer
645 Verlag.
- 646 Müller, H., Liedtke, H. C., Menegon, M., Beck, J., Ballesteros-Mejia, L., Nagel, P., & Loader, S.
647 P. (2013). Forests as promoters of terrestrial life-history strategies in East African
648 amphibians. *Biology Letters*, 9(3), 20121146.
- 649 Naumann, B., & Englert, C. (2018). Dispersion/reaggregation in early development of annual
650 killifishes: Phylogenetic distribution and evolutionary significance of a unique feature.
651 *Developmental Biology*, 442(1), 69-79.
- 652 Olsson, L., Moury, D. J., Carl, T. F., Håstad, O., & Hanken, J. (2002). Cranial neural crest-cell
653 migration in the direct-developing frog, *Eleutherodactylus coqui*: molecular heterogeneity
654 within and among migratory streams. *Zoology*, 105(1), 3-13.
- 655 Palenstijn, W. J., Batenburg, K. J., & Sijbers, J. (2011). Performance improvements for iterative
656 electron tomography reconstruction using graphics processing units (GPUs). *Journal of*
657 *Structural Biology*, 176(2), 250-253. doi:10.1016/j.jsb.2011.07.017
- 658 Quinzio, S. I., & Goldberg, J. (2019). Transient integumentary structures in *Boana riojana*
659 (Anura, Hylidae) tadpoles. *Amphibia-Reptilia*, 40(4), 543-549.
- 660 Robinson, D. H., & Heintzelman, M. B. (1987). Morphology of ventral epidermis of *Rana*
661 *catesbeiana* during metamorphosis. *The Anatomical Record*, 217(3), 305-317.
- 662 San Mauro, D., Gower, D. J., Müller, H., Loader, S. P., Zardoya, R., Nussbaum, R. A., &
663 Wilkinson, M. (2014). Life-history evolution and mitogenomic phylogeny of caecilian
664 amphibians. *Molecular Phylogenetics and Evolution*, 73, 177-189.

- 665 Schlosser, G. (2008). Development of the retinotectal system in the direct-developing frog
666 *Eleutherodactylus coqui* in comparison with other anurans. *Frontiers in Zoology*, 5(1), 9.
- 667 Schlosser, G., Kintner, C., & Northcutt, R. G. (1999). Loss of ectodermal competence for lateral
668 line placode formation in the direct developing frog *Eleutherodactylus coqui*.
669 *Developmental biology*, 213(2), 354-369.
- 670 Schlosser, G., & Roth, G. (1997). Evolution of nerve development in frogs; pp. 94–112. *Brain,*
671 *Behavior and Evolution*, 50(2), 94-112.
- 672 Schluter, D., Clifford, E. A., Nemethy, M., & McKinnon, J. S. (2004). Parallel evolution and
673 inheritance of quantitative traits. *The American Naturalist*, 163(6), 809-822.
- 674 Schneider, C. A., Rasband, W. S., & Eliceiri, K. W. (2012). NIH Image to ImageJ: 25 years of
675 image analysis. *Nature Methods*, 9(7), 671-675.
- 676 Schreiber, A. M., & Brown, D. D. (2003). Tadpole skin dies autonomously in response to thyroid
677 hormone at metamorphosis. *Proceedings of the National Academy of Sciences*, 100(4),
678 1769-1774.
- 679 Schweiger, S., Naumann, B., Larson, J. G., Möckel, L., & Müller, H. (2017). Direct development
680 in African squeaker frogs (Anura: Arthroleptidae: *Arthroleptis*) reveals a mosaic of
681 derived and plesiomorphic characters. *Organisms Diversity & Evolution*, 17(3), 693-707.
- 682 Schweiger, S., Naumann, B., & Müller, H. (in prep.). The ghost of the tadpole - Embryonic
683 development of the cranial musuloskeletal system in African squeaker frogs (*Arthroleptis*)
684 reveals heterochronic shifts and parallel evolution of differential metamorphosis in direct
685 developing frogs.
- 686 Shi, Y.-B. (1999). *Amphibian metamorphosis: from morphology to molecular biology*: Wiley-
687 Liss.
- 688 Simpson, G. G. (1961). Principles of animal taxonomy.
- 689 Smith-Gill, S. J., & Carver, V. (1981). Biochemical characterization of organ differentiation and
690 maturation. In *Metamorphosis* (pp. 491-544): Springer.
- 691 Smith, A. (1849). *Illustrations of the Zoology of South Africa: Consisting Chiefly of Figures and*
692 *Descriptions of the Objects of Natural History Collected During an Expedition Into the*
693 *Interior of South Africa, in the Years 1834, 1835, and 1836; Fitted Out by" the Cape of*
694 *Good Hope Association for Exploring Central Africa"* (Vol. 4).

- 695 Tamakoshi, T., Oofusa, K., & Yoshizato, K. (1998). Visualization of the initiation and sequential
696 expansion of the metamorphic conversion of anuran larval skin into the precursor of adult
697 type. *Development, Growth & Differentiation*, 40(1), 105-112.
- 698 Tata, J. R. (2006). Amphibian metamorphosis as a model for the developmental actions of
699 thyroid hormone. *Molecular and Cellular Endocrinology*, 246(1-2), 10-20.
- 700 ten Brink, H. t., Onstein, R. E., & de Roos, A. M. (2020). Habitat deterioration promotes the
701 evolution of direct development in metamorphosing species. *Evolution*.
- 702 Thibaudeau, G., & Altig, R. (1999). Endotrophic anurans: development and evolution. *Tadpoles:
703 the Biology of Anuran Larvae*, 170-188.
- 704 Thomas, R. (1966). New species of antillean *Eleutherodactylus*. *Quarterly Journal of the Florida
705 Academy of Sciences*, 28(4), 375-391.
- 706 Townsend, D. S., & Stewart, M. M. (1985). Direct development in *Eleutherodactylus coqui*
707 (Anura: Leptodactylidae): a staging table. *Copeia*, 423-436.
- 708 van Aarle, W., Palenstijn, W. J., Cant, J., Janssens, E., Bleichrodt, F., Dabravolski, A., . . .
709 Sijbers, J. (2016). Fast and flexible X-ray tomography using the ASTRA toolbox. *Optics
710 Express*, 24(22), 25129-25147. doi:Doi 10.1364/Oe.24.025129
- 711 van Aarle, W., Palenstijn, W. J., De Beenhouwer, J., Altantzis, T., Bals, S., Batenburg, K. J., &
712 Sijbers, J. (2015). The ASTRA Toolbox: A platform for advanced algorithm development
713 in electron tomography. *Ultramicroscopy*, 157, 35-47. doi:10.1016/j.ultramic.2015.05.002
- 714 Varga, J. F., Bui-Marinis, M. P., & Katzenback, B. A. (2019). Frog skin innate immune
715 defences: sensing and surviving pathogens. *Frontiers in Immunology*, 9, 3128.
- 716 Verma, K. (1965). Regional differences in skin gland differentiation in *Rana pipiens*. *Journal of
717 Morphology*, 117(1), 73-85.
- 718 Wake, D., & Hanken, J. (1996). Direct development in the lungless salamanders: what are the
719 consequences for developmental biology, evolution and phylogenesis? *International
720 Journal of Developmental Biology*, 40(4), 859-869.
- 721 Wilde, F., Ogurreck, M., Greving, I., Hammel, J. U., Beckmann, F., Hipp, A., . . . Schreyer, A.
722 (2016). Micro-CT at the imaging beamline P05 at PETRA III. *AIP Conference
723 Proceedings*, 1741(1), 030035. doi:10.1063/1.4952858
- 724 Yasutomi, M. (1987). Migration of epidermal melanophores to the dermis through the basement
725 membrane during metamorphosis in the frog, *Rana japonica*. *Pigment cell research*, 1(3),
726 181-187.

727 Yoshizato, K. (1992). Death and transformation of larval cells during metamorphosis of anura.

728 *Development, growth and differentiation*, 34(6), 607-612.

729 Ziermann, J. M., & Diogo, R. (2014). Cranial muscle development in frogs with different

730 developmental modes: direct development versus biphasic development. *Journal of*

731 *morphology*, 275(4), 398-413.

732

733

734 **Figure legends**

735

736 Figure 1. A, a family-level phylogeny of recent frogs based on Feng et al., 2017 (Feng et al.,
737 2017). Blue boxes indicate the presence of an ancestral biphasic live history while orange boxes
738 indicate direct development. B, a schematic graph showing the gradual morphological change
739 during ontogeny of the direct developing *Arthroleptis* (*A. wahlbergii*; 1, embryo; 2, adult frog)
740 and the more climactic metamorphic change in its biphasic sister genus *Cardioglossa* (*C.*
741 *manengouba*; 1, tadpole; 2, adult frog). Photographs are not to scale. C, schematic diagrams of
742 the organization of the tadpole and adult frog skin.

743

744 Figure 2. A-G, Photographs of the skin pigmentation of different developmental stages of
745 *Arthroleptis wahlbergii*. The schematic embryo on the left illustrates the photographed regions
746 (1, 2 and 3). Blue arrows indicate the position of the eye, red asterisks the position of the
747 forelimb. The dotted grey lines and percentage number indicate the distance between the back
748 (dorsal, 0%) and ventral midline (ventral, 100%). The black arrow in A2-D2 indicates the
749 migration distance of the first melanophore type (shown in B`). The white arrow in H2-J2
750 indicates the migration distance of the second melanophore type (shown in G`). The black dotted
751 line in C3-G3 indicates the ventral midline. Scale bar is 200 μ m.

752

753 Figure 3. Histological cross sections of the skin of *Arthroleptis wahlbergii* at different
754 developmental stages. The schematic embryo on top illustrates the photographed regions (1-5).
755 Grey arrows indicate the epidermal cilia. Yellow arrows indicate intracellular yolk droplets.

756 Black arrows indicate epidermal nuclei. The yellow arrow in H3 indicates the glandular duct. The
757 number of epidermal cellular layers is indicated by a grey line and asterisks. Scale bar is 20 μm .
758 cc, ciliated cell; co, stratum corneum; ec, epithel cell; etm, epaxonic trunk muscles; g,
759 multicellular gland progenitor; g1, unicellular gland; g2, multicellular granular gland; g3,
760 multicellular mucus gland; htm, hypaxonic trunk muscles; m, mesenchyme; me, melanophore; sc,
761 stratum compactum; sp, stratum spongiosum; vc, vacuole.

762
763 Figure 4. Fluorescent PCNA antibody staining in cross sections through the skin of *Arthroleptis*
764 *wahlbergii* embryos at different developmental stages. Two different antibodies against PCNA
765 have been used. PCNA-1 is colored in yellow and shown in A, C, E and G. PCNA-2 is colored in
766 magenta and shown in B, D, F and H. Nuclei are stained with DAPI and colored in grey. A` and
767 B` Show a close up of the PCNA signal within the nucleus. Magenta arrows in B indicate the
768 scattered antibody signal. A-H, scale bar is 20 μm . A` and B`, scale bar is 10 μm . g2,
769 multicellular granular gland; g3, multicellular mucus gland.

770
771 Figure 5. A-C volume renderings of μCT scans of different developmental stages of *Arthroleptis*
772 *xenodactyloides*. The thyroid glands are colored in lilac. Renderings are not to scale. D-H,
773 histological cross-sections of the ventral head region of *A. wahlbergii* embryos at different
774 developmental stages. Blue arrows indicate absence of colloid within follicles. Blue asterisks
775 indicate the presence of colloid within follicles. Scale bar is 25 μm . hp, hyoid plate; th, thyroid
776 gland.

777

778 Figure 6. A, schematic illustration of thyroid gland follicles and the measured parameters. B, Box
779 plot of the follicle cell height in *Arthroleptis* at different developmental stages. C, diagram of the
780 follicle number in *Arthroleptis* at different developmental stages. D, diagram of the average
781 follicle diameter in *Arthroleptis* at different developmental stages. Aw, *A. wahlbergii*; Ax, *A.*
782 *xenodactyloides*.

783
784 Figure 7. A, histological cross sections of the skin of a *Cardioglossa manengouba* tadpole at
785 Gosner-stage 27. The schematic tadpole on top illustrates the photographed regions (1-5). Black
786 arrows indicate epidermal nuclei. The number of epidermal cellular layers is indicated by a grey
787 line and asterisks. B, volume renderings of a synchrotron scan of a *C. manengouba* tadpole at
788 Gosner-stage 27. The thyroid glands are colored in lilac. Renderings are not to scale. C,
789 histological cross sections of the ventral head region of the same tadpole as in A. Lilac arrows
790 indicate absence of colloid within follicles. Scale bar is 20 μm . bh, basihyal; ch, ceratohyal; co,
791 keratinized layer; ec, epithel cell; g1, unicellular gland; htm, hypaxonic trunk muscles; m,
792 mesenchyme; me, melanophore; mu, muscle; sc, stratum compactum; th, thyroid gland.

793
794 Figure 8. Schematic summary of the skin composition of *Arthroleptis* at different developmental
795 stages. Presumptive thyroid gland activity inferred from histological measurements is indicated in
796 lilac.

797
798 Supplementary material 1. Specimen list. ICH, immune-histochemistry; MB-aF, Methylene blue
799 acidic Fuchsin; PMC, polymolybdenic acid; μCT , micro-computed tomography.

800

801 Supplementary material 2. Adult skin histology. Histological cross sections of the skin of an adult
802 (1.3 cm) *Arthroleptis wahlbergi*. A, dorsal head region. B, lateral head region. The orange arrow indicates
803 the glandular duct. C, ventral head region. The number of epidermal cellular layers is indicated by a grey
804 line and asterisks. Scale bar is 20 μm . co, stratum corneum; ec, epithel cell; g2, multicellular granular
805 gland; g3, multicellular mucus gland; me, melanophore; sc, stratum compactum; sp, stratum spongiosum.

Figure 1

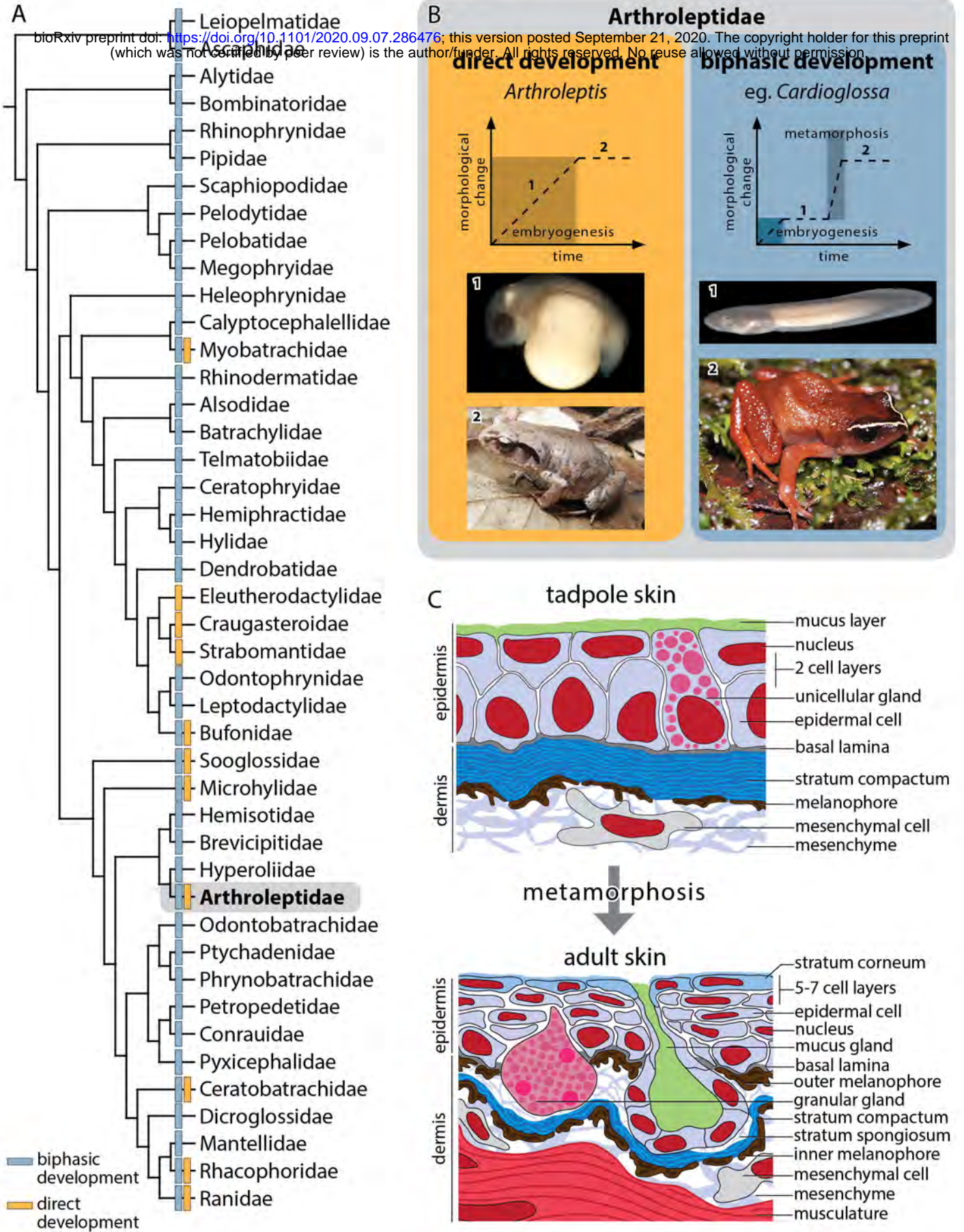


Figure 2

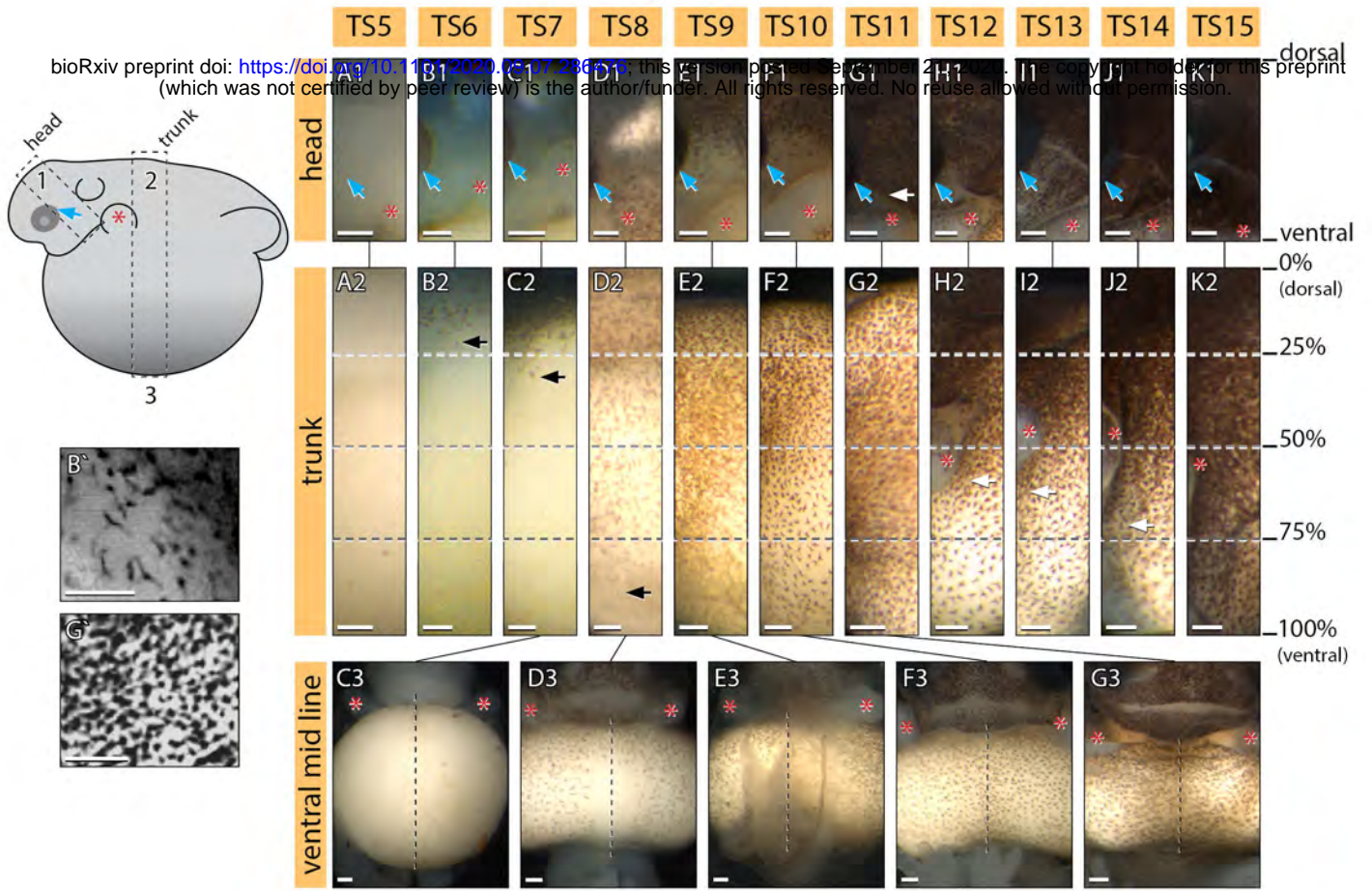


Figure 3

bioRxiv preprint doi: <https://doi.org/10.1101/2020.09.07.286476>; this version posted September 21, 2020. The copyright holder for this preprint (which was not certified by peer review) is the author/funder. All rights reserved. No reuse allowed without permission.

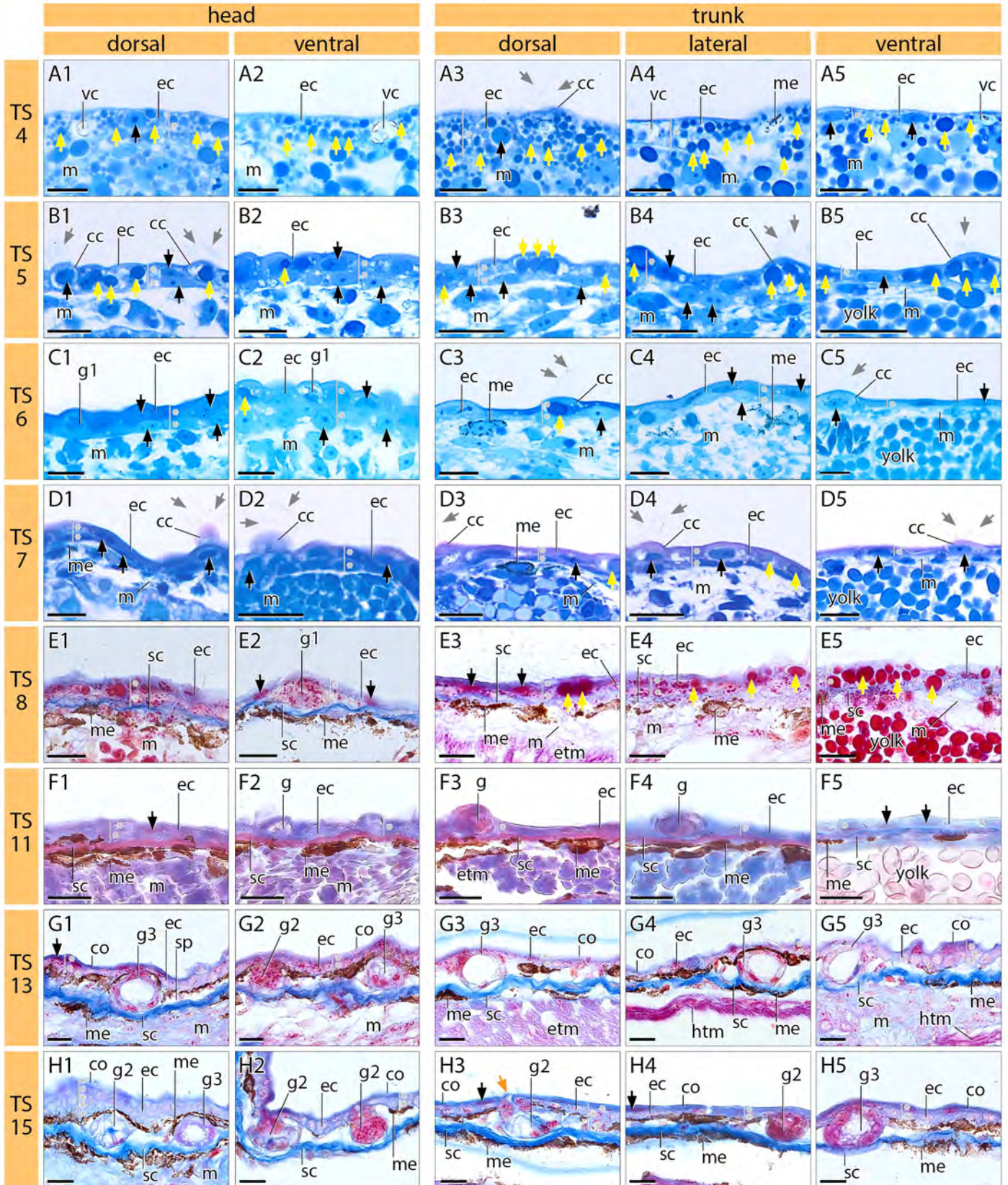
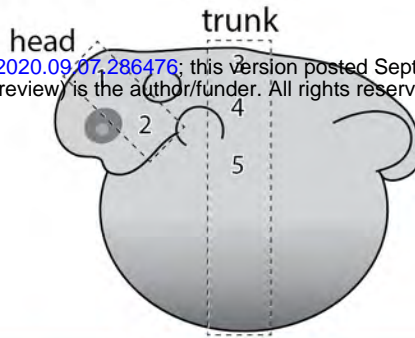


Figure 4

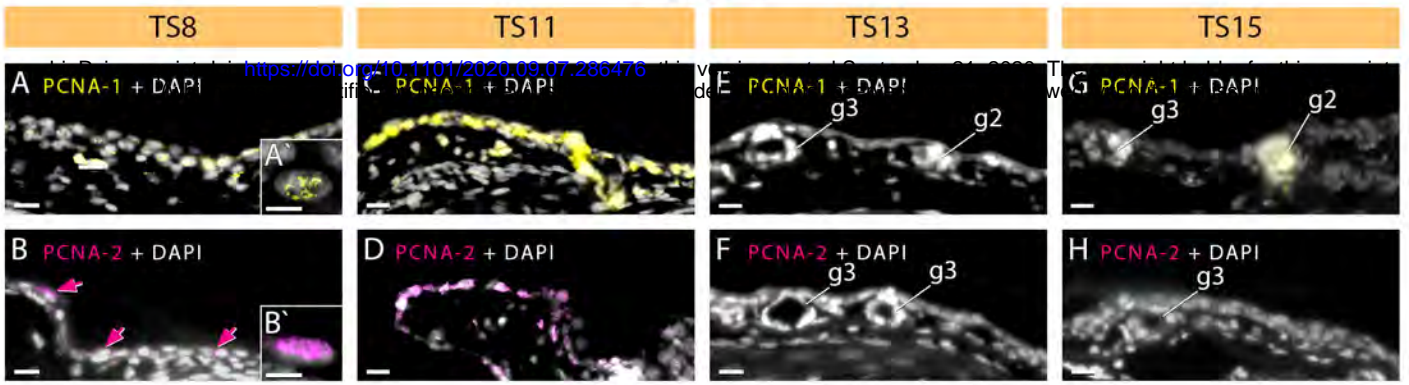


Figure 5

bioRxiv preprint doi: <https://doi.org/10.1101/2020.09.07.286476>; this version posted September 21, 2020. The copyright holder for this preprint (which was not certified by peer review) is the author/funder. All rights reserved. No reuse allowed without permission.

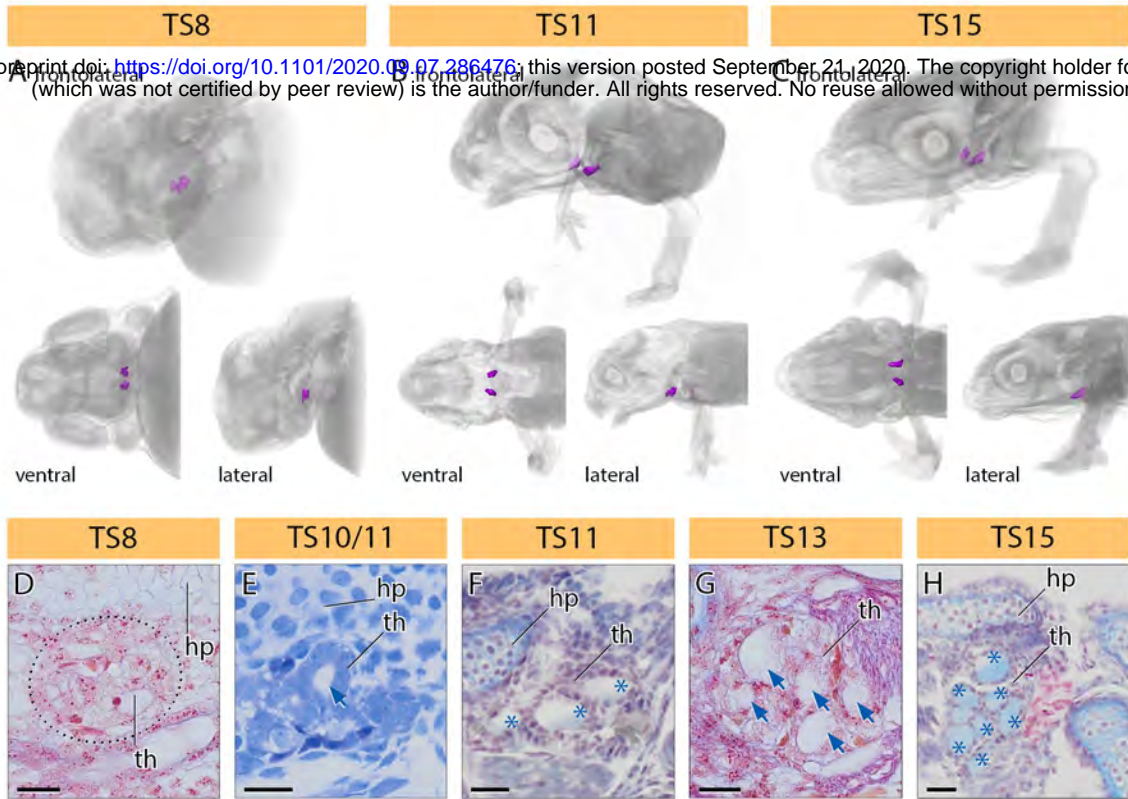


Figure 6

bioRxiv preprint doi: <https://doi.org/10.1101/2020.09.07.286476>; this version posted September 21, 2020. The copyright holder for this preprint (which was not certified by peer review) is the author/funder. All rights reserved. No reuse allowed without permission.

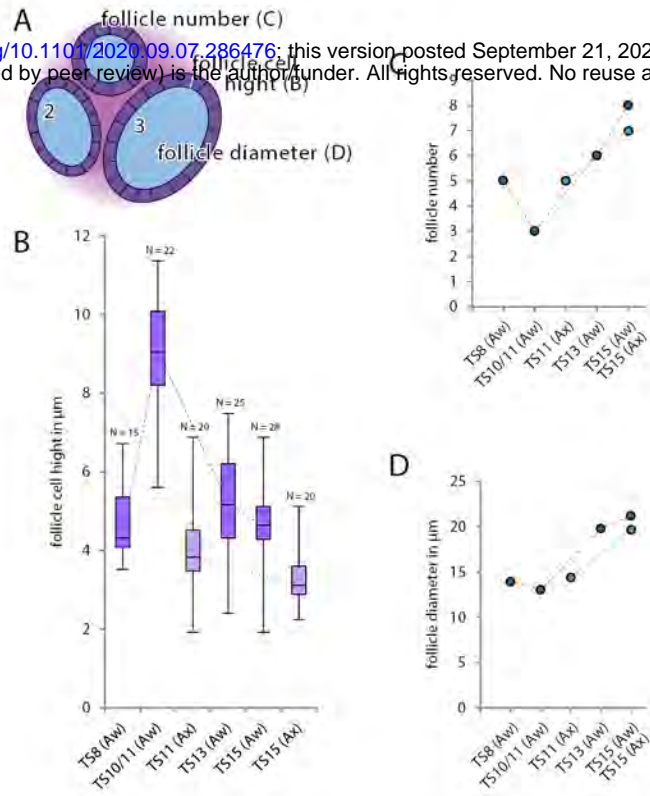


Figure 7

bioRxiv preprint doi: <https://doi.org/10.1101/2020.09.07.286476>; this version posted September 21, 2020. The copyright holder for this preprint (which was not certified by peer review) is the author/funder. All rights reserved. No reuse allowed without permission.

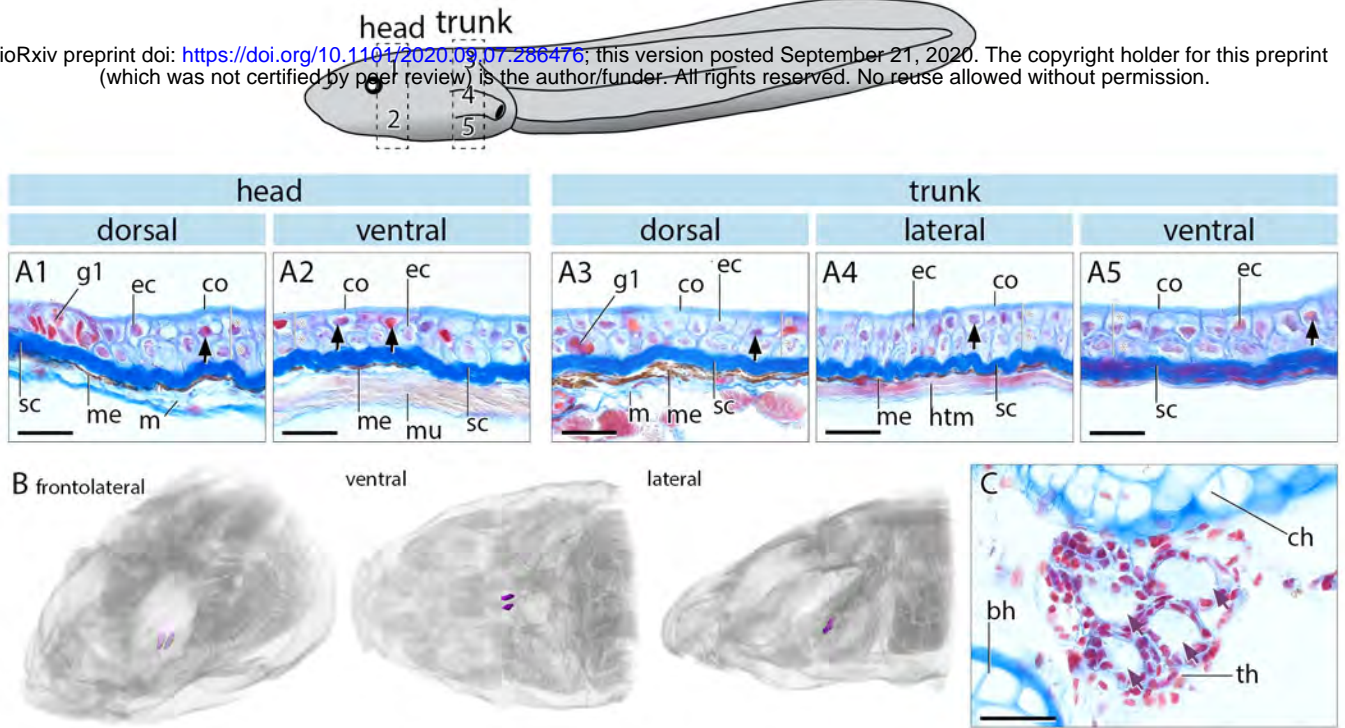
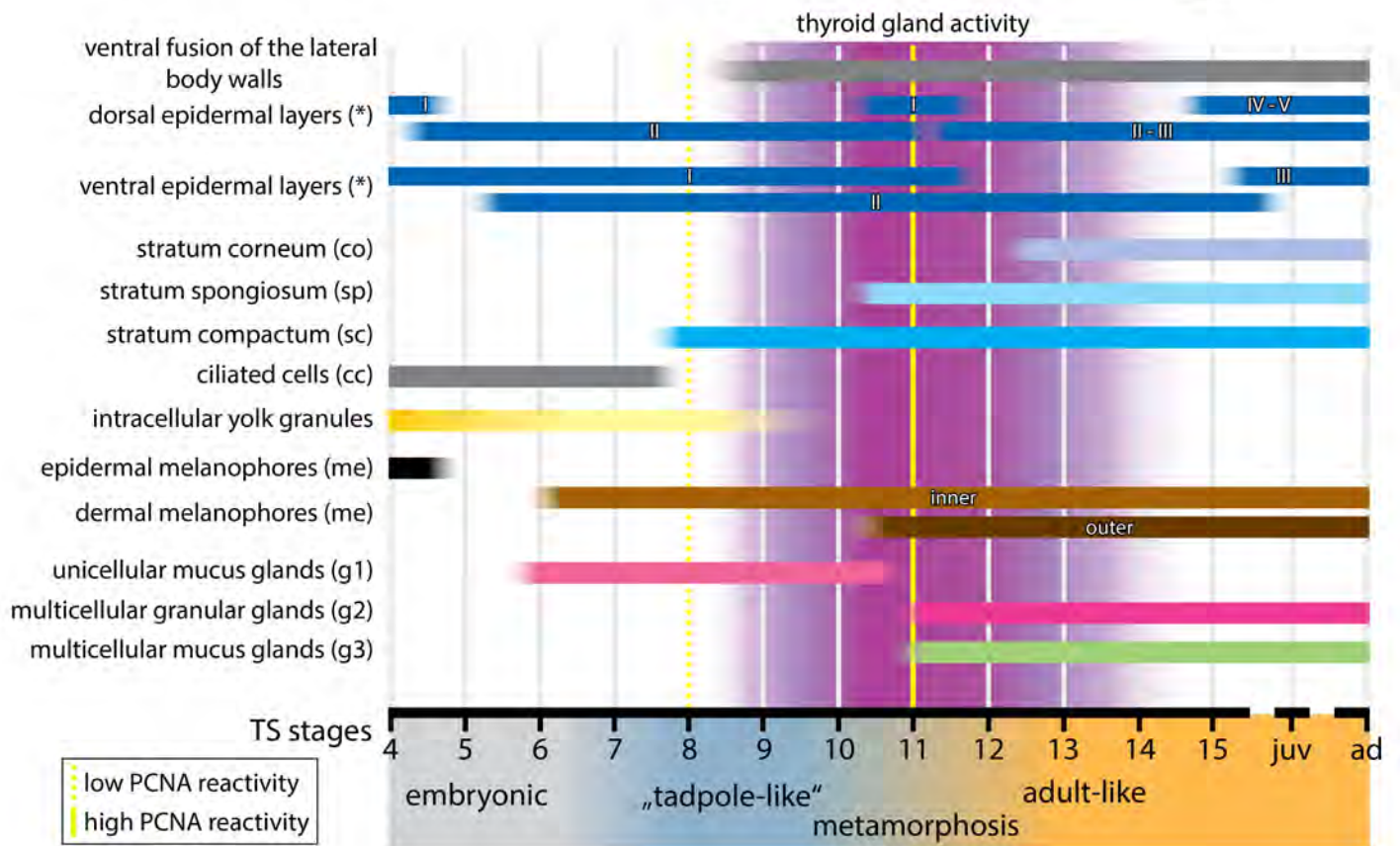


Figure 8

bioRxiv preprint doi: <https://doi.org/10.1101/2020.09.07.286476>; this version posted September 21, 2020. The copyright holder for this preprint (which was not certified by peer review) is the author/funder. All rights reserved. No reuse allowed without permission.



Supplementary material 1

bioRxiv preprint doi: <https://doi.org/10.1101/2020.09.07.286476>; this version posted September 21, 2020. The copyright holder for this preprint (which was not certified by peer review) is the author/funder. All rights reserved. No reuse allowed without permission.

ID	TS stage	species	technique	staining
#01	3	<i>A. wahlbergii</i>	photo	
#02	4	<i>A. wahlbergii</i>	histology/photo	MB-aF/ -
#03	5	<i>A. wahlbergii</i>	histology/photo	MB-aF/ -
#04	5/6	<i>A. wahlbergii</i>	photo	-
#05	5/6	<i>A. wahlbergii</i>	photo	-
#06	6	<i>A. wahlbergii</i>	histology/photo	MB-aF/ -
#07	6/7	<i>A. wahlbergii</i>	photo	-
#08	7	<i>A. xenodactyloides</i>	histology	MB-aF
#09	7	<i>A. wahlbergii</i>	photo	-
#10	8	<i>A. xenodactyloides</i>	μCT	1% PMA
#11	8	<i>A. wahlbergii</i>	histology/ICH	MB-aF/anti-PCNA
#12	8	<i>A. wahlbergii</i>	photo	-
#13	8	<i>A. wahlbergii</i>	photo	-
#14	9	<i>A. xenodactyloides</i>	histology	MB-aF
#15	9	<i>A. wahlbergii</i>	photo	-
#16	10	<i>A. wahlbergii</i>	photo	-
#17	10	<i>A. wahlbergii</i>	photo	-
#18	11	<i>A. xenodactyloides</i>	μCT	1% PMA
#19	11	<i>A. xenodactyloides</i>	histology	Azan
#20	11	<i>A. wahlbergii</i>	histology/ICH	Azan/anti-PCNA
#21	11	<i>A. wahlbergii</i>	photo	-
#22	11	<i>A. wahlbergii</i>	photo	-
#23	11/12	<i>A. wahlbergii</i>	photo	-
#24	12	<i>A. wahlbergii</i>	photo	-
#25	12	<i>A. wahlbergii</i>	photo	-
#26	12/13	<i>A. wahlbergii</i>	photo	-
#27	13	<i>A. xenodactyloides</i>	histology	Azan
#28	13	<i>A. wahlbergii</i>	histology/ICH	Azan/anti-PCNA
#29	13	<i>A. wahlbergii</i>	photo	-
#30	13	<i>A. wahlbergii</i>	photo	-
#31	14	<i>A. wahlbergii</i>	photo	-
#32	14/15	<i>A. wahlbergii</i>	photo	-
#33	15	<i>A. xenodactyloides</i>	μCT	1% PMA
#34	15	<i>A. xenodactyloides</i>	histology	Azan
#35	15	<i>A. wahlbergii</i>	histology/ICH	Azan/anti-PCNA
#36	15	<i>A. wahlbergii</i>	photo	-
#37	15	<i>A. wahlbergii</i>	photo	-
#38	15	<i>A. wahlbergii</i>	photo	-
#39	adult, 1.3 cm	<i>A. wahlbergii</i>	histology	Azan
#40	adult, 2 cm	<i>A. wahlbergii</i>	histology	Azan
#41	tadpole	<i>Cardioglossa</i> sp.	histology	Azan

Supplementary material 2

